

# Effects of Higher Order and Long-Range Synchronizations for Classification and Computing in Oscillator-Based Spiking Neural Networks

Andrey Velichko\*, Vadim Putrolaynen, and Maksim Belyaev

Petrozavodsk State University, Petrozavodsk, 185910, Russia

\* Corresponding author: e-mail velichko@petrsu.ru

## Abstract

Development of artificial oscillator-based spiking neural networks (SNN), which are able to solve effectively various cybernetics problems including image recognition and adaptive control, is a key line of research. We have thoroughly explored the scheme of two thermally coupled VO<sub>2</sub> oscillators and found its effect of high order synchronization (HOS), which may be used to increase SNN classification capacity  $N_s$ . Phase-locking estimation method has been developed to determine values of subharmonic ratio  $SHR$  and synchronization effectiveness  $\eta$ . The experimental scheme has  $N_s=12$  and  $SHR$  distributions are shaped as Arnold's tongues. In a model  $N_s$  may reach maximum of  $N_s>150$  at certain levels of coupling strength and noise. We demonstrate the long-range synchronization effect in a one-dimensional chain of oscillators and the phenomenon of synchronization transfer even at low values of  $\eta$  for intermediate links. The paper demonstrates realization of analogue operation of "multiplication", synchronize-based logic for binary computations, and possibility of development of the interface between SNN and computer. The described effects increasing classification capacity of oscillator schemes and calculation principles based on the universal physical effect - HOS may be applied for any spiking type oscillators with any coupling type therefore enhancing practical value of the presented results to expand SNN capabilities.

**Keywords:** vanadium dioxide; oscillatory neural networks; thermal coupling; higher order synchronization; classification; oscillator based computing

## 1. Introduction

Currently substantial progress has been achieved in studying and understanding of synchronization and desynchronization processes in networks of interacting oscillators [1]. The results of these studies have been used to solve a wide variety of applied tasks, for instance, pattern recognition [2–4], information classification [5–7] and computational operations [8–11]. Various oscillator schemes have been suggested for this purpose based on different physical phenomena: oxide-based oscillators [12–15], nanomechanical oscillators [11,16], spin-torque nano-oscillators [8,17–20], laser oscillators [21] and superconducting oscillators [22].

A real biological neuron is a complex biochemical system operating with ceaseless multichannel voltage impulses – spikes [23]. Spikes sequences come to neuron synapses and the neuron itself also generates a sequence of spikes at the output that spread along its axon. The purpose of neuron modeling is research of its real neurophysiology, but in the area of cybernetics and computer science oriented on practical applications the urgent issue is to find which features of biological neurons enable neural networks to solve such important tasks as pattern recognition, adaptive control and long-range synchronization whose character is open to discussion among scholars [24–26] and which features of a real biological neuron may be ignored when modeling to construct fast and effective artificial neural networks.

A model of VO<sub>2</sub> spiking neural networks (SNN) [27–29] is developing rapidly because oscillators with VO<sub>2</sub>-based switches that have the shape of current peaks resembling that of real neural spikes may be easily realized. In addition, there is always inner noise in a VO<sub>2</sub>-based oscillator scheme due to instability of threshold characteristics of a switching channel [30,31]. It is known that introduction of noise into spike models is reasonable because there are a lot of noise effect sources in a real neuron [32,33], for instance, release probability of inlet spikes on synapses [34]. In this study we also used VO<sub>2</sub>-structures as experimental and model objects and mechanism of two oscillators interaction was realized through thermal coupling described recently in our work [35,36]. The advantage of this type of coupling over capacity or resistive couplings is that oscillators are completely isolated from each other both for alternative and direct currents [37] thus preventing operating points displacement and improving their stability with varying control parameters.

We show that spike oscillations possess a wide line spectrum of frequencies, besides, separate spikes in each circuit appear in-phase at oscillators interaction resulting in phase-locking effect. These features cause a pronounced effect of higher order synchronization [1] manifested in oscillations synchronization at separate spectrum subharmonics. Nevertheless, it is worth noting that this effect is studied insufficiently when problems of its application to classification and pattern recognition tasks in SNN are considered.

The problem of synchronization state identification is being widely discussed in literature. Lowet *et al.* [38] compare two basic approaches - spectral coherence and phase-locking value ones – and come to the conclusion that phase-locking value approach is more preferable in most cases especially in those of strong noise and partially (intermittent) synchronized state. Here we present and discuss an alternative effective algorithm which we have developed before [36] that enables us to determine and evaluate the effect of high order synchronization. Moreover, we show the link between spectral coherence and phase-locking value approaches and discuss the advantages of the latter.

The main objective of the research was to study the effect of high order synchronization and the possibility of its usage to increase the classification capacity of oscillator-based spiking neural networks. The problem of classification is closely linked with the pattern recognition problem that is also being studied intensively nowadays. Vodenicarevic *et al.* [5] suggested a scheme on the basis of four-coupled oscillators and showed that it is sturdy against noise effect, parameters variation and oscillator non-linearity and also it possesses over nine stable states. In our work, we suggest an alternative approach to this problem solution that may result in increasing classification capacity of oscillator schemes at less number of oscillators.

Systems of coupled oscillators are also used for non-Boolean calculus (analog logic) [3,4,8,39,40] where input parameters are given via physical characteristics of a scheme, for instance, via oscillator frequency, phase differential or force of their coupling. Output data of such a system are also physical characteristics of a scheme in its final stable state. Because dynamics of each separate element operation changes simultaneously calculations in analog oscillator systems require parallel information processing, its scope depends on the number of oscillators in the network and allows considerable simplification of calculations with floating point numbers. A well-known phase-based logic involving oscillator usage was suggested by John von Neumann [41], and this idea is still being studied. For instance, Roychowdhury [42] demonstrated its advantages in comparison with level-based CMOS computing such as high noise resistance and low energy consumption. In this work, we have tried to develop the principles of calculations based on effect of high order synchronization and suggest our version of synchronization-based logic.

## 2. Methods

### 2.1 Experimental techniques

We have described in detail the process of VO<sub>2</sub> films deposition and VO<sub>2</sub> films-based planar structures in our previous paper [35]. Coupled structures (Fig. 1a) were formed with the distances of  $d \sim 12 \mu\text{m}$  and  $d \sim 21 \mu\text{m}$  to ensure strong and weak thermal couplings between them, respectively [36,43]. It should be noted that the maximum temperature induced from a neighboring switch was  $\Delta T^p \sim 0.7 \text{ K}$  at strong coupling and  $\Delta T^p \sim 0.2 \text{ K}$  at weak coupling. I-V characteristics of switches coincided and were of typical shape shown in Fig. 1b. The basic parameters of I-V characteristic are threshold currents ( $I_{th}$ ,  $I_h$ ), threshold voltages ( $U_h$ ,  $U_{th}$ ), cutoff voltage ( $U_{cf}$ ) and dynamic resistances at high and low states ( $R_{off}$  и  $R_{on}$ ). More detailed description of structure characteristics and thermal coupling is given in our papers [44–46].

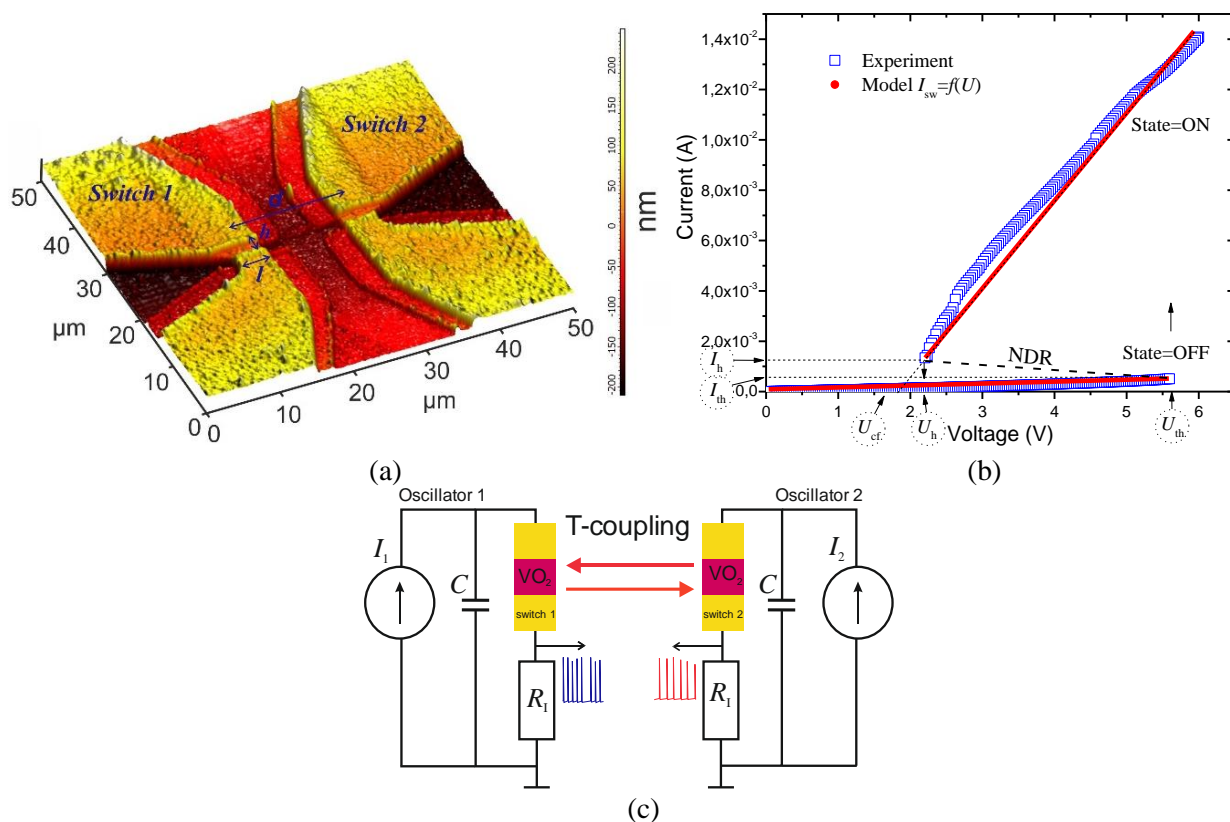


**Figure 1** [Color online] AFM image of coupled planar VO<sub>2</sub>-structures (a), typical experimental I-V characteristic of a separate switch (b, Experiment curve) and its model curve (b, Model curve). Experimental (c) scheme of two oscillators with thermal coupling. Length  $l$  and gap  $h$  of the switch interelectrode space were  $\sim 3\text{-}4 \mu\text{m}$  and  $2.5 \mu\text{m}$ , respectively.

Experimental scheme of oscillator circuits is presented in Fig. 1c. The scheme of each circuit has a current source  $I_{1(2)}$  capacity  $C$  (100 nF) and limiting current resistor  $R_1$  (250  $\Omega$ ) connected in series with VO<sub>2</sub>-switch. Output current signal was registered from resistor  $R_1$ . Oscillations in a single circuit are studied well [3,29,31,37,47] and are observed when the current of power supply is within the range of  $I_{th} < I_{1(2)} < I_h$ . This condition ensures that the scheme operating point is in NDR area (Fig. 1b). Nevertheless, when two circuits have a strong coupling [48], low boundaries of current range for oscillations widen. This is due to the fact that at reciprocal Joule heating the threshold voltage  $U_{th}$  decreases by the value of coupling strength  $\Delta$  (see the model below) and therefore causes decrease of  $I_{th}$ .

The study of oscillation dynamics was performed with a four-channel oscilloscope Picoscope 5442B with the maximum sampling rate of 125 MS/sec in 14-bit mode. A two-channel sourcemeter Keythley 2636A was used for the DC I-V characteristic measurements (sweeping rate 1V/s), and also as an oscillatory circuit current source.

A surface morphology characterization was conducted using AFM NTEGRA Prima in non-contact mode.

## 2.2 Model of an oscillator and thermal coupling

The model scheme for current (voltage) oscillogram calculation in couples oscillator circuits is shown in Fig. 2. It duplicates the experimental scheme except for a current resistor but includes a controlled noise generator  $U_n$ . Included  $U_n$  allows modeling of scheme real inside noise occurring because of current channel fluctuations in the switch structure [30,49] and analyzing the influence of outside noise amplitude on the characteristics of synchronization effect.

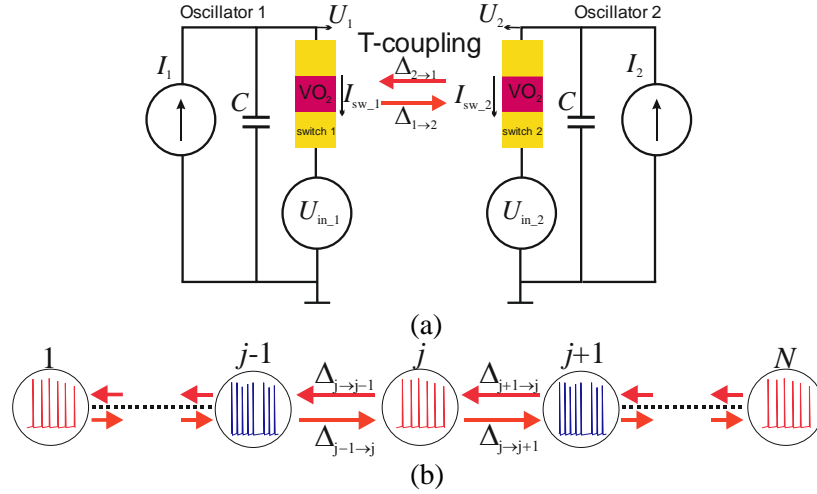


**Figure 2** [Color online] Model schemes of two oscillators with thermal coupling (a) and  $N$ - oscillators chain (b).

To calculate the model scheme a simple system of differential equations was solved:

$$\begin{cases} C \frac{dU_1(t)}{dt} = I_1 - I_{sw,1}(t), \text{ where } I_{sw,1}(t) = f(U_1(t) - U_n(t)) \\ C \frac{dU_2(t)}{dt} = I_2 - I_{sw,2}(t), \text{ where } I_{sw,2}(t) = f(U_2(t) - U_n(t)) \end{cases}, \quad (1)$$

where  $U_{1(2)}(t)$  is voltage at capacitors,  $I_{1(2)}$  is power current of constant value,  $I_{sw,1(2)}(t)$  is current via switches and  $(U_{1(2)}(t) - U_n(t))$  is voltage at switches at the corresponding circuits, function  $f(U)$  is determined by linear I-V characteristic of structure (2-3). In this case, the parameters of I-V characteristic depend on the state of the neighbor switch (4). Equation (1) was numerically calculated with respect to time at regular intervals  $\Delta t = 10^{-5}$  s using implicit Euler method and discrete noise  $U_n(t)$  was generated according to the algorithm [48]  $U_n(t) = U_{n0} \cdot \text{randn}(t)$ , where  $U_{n0}$ - noise amplitude and  $\text{randn}(t)$  – normal random numbers generator with zero mean and dispersion equal to 1.

To form the function  $f(U)$  both branches of I-V characteristic (Fig. 1b, Model curve) were approximated by straight-line segments with dynamic resistances  $R_{off}$  and  $R_{on}$ :

$$f(U) = \begin{cases} \frac{U}{R_{off}}, & \text{if } State = \text{OFF} \\ \frac{(U - U_{cf})}{R_{on}}, & \text{if } State = \text{ON} \end{cases}, \quad (2)$$

where “State” denotes the switch state (OFF- high, ON – low).

Transitions from one state into another for two switches ( $State_1$  and  $State_2$ ) were modeled according to the following algorithm:

$$\begin{aligned}
State_1 &= \begin{cases} \text{OFF,} & \text{if } (State_1 = \text{ON}) \text{ and } (U_1 < U_h) \\ \text{ON,} & \text{if } (State_1 = \text{OFF}) \text{ and } (U_1 > U_{th,1}) \end{cases}, \\
State_2 &= \begin{cases} \text{OFF,} & \text{if } (State_2 = \text{ON}) \text{ and } (U_2 < U_h) \\ \text{ON,} & \text{if } (State_2 = \text{OFF}) \text{ and } (U_2 > U_{th,2}) \end{cases}
\end{aligned} \tag{3}$$

where  $U_{th,1}$  and  $U_{th,2}$  are threshold turn-on voltages of switches according to the algorithm:

$$\begin{aligned}
U_{th,1} &= \begin{cases} U_{th} - \Delta_{2 \rightarrow 1}, & \text{if } State_2 = \text{ON} \\ U_{th}, & \text{if } State_2 = \text{OFF} \end{cases}, \\
U_{th,2} &= \begin{cases} U_{th} - \Delta_{1 \rightarrow 2}, & \text{if } State_1 = \text{ON} \\ U_{th}, & \text{if } State_1 = \text{OFF} \end{cases},
\end{aligned} \tag{4}$$

where  $\Delta_{1 \rightarrow 2}$  and  $\Delta_{2 \rightarrow 1}$  (coupling strength) determine the degree of one switch impact on the other one at thermal coupling (Fig. 2a). For instance, the value  $\Delta_{1 \rightarrow 2}$  shows how the threshold voltage value  $U_{th,2}$  (switch 2) changes at the switch 1 transition into a low state. Thus oscillators interaction occurs due to their mutual effect on threshold characteristics and such cases may be found in literature [1,50]. But our scheme has no electric coupling of oscillators therefore the equation (1) is much simplified and allows easy network modeling with larger number of coupled oscillators.

To study the effect of long-range synchronization for a N-oscillators chain we used the model shown in Fig. 2b where the interaction of only two neighbor oscillators was taken into account and  $U_{th,j}$  of each oscillator inside the chain was determined according to the following algorithm:

$$U_{th,j} = \begin{cases} U_{th,j} - \Delta_{j-1 \rightarrow j}, & \text{if } (State_{j-1} = \text{ON}) \text{ and } (State_{j+1} = \text{OFF}) \\ U_{th,j} - \Delta_{j+1 \rightarrow j}, & \text{if } (State_{j-1} = \text{OFF}) \text{ and } (State_{j+1} = \text{ON}) \\ U_{th,j} - \Delta_{j-1 \rightarrow j} - \Delta_{j+1 \rightarrow j}, & \text{if } (State_{j-1} = \text{ON}) \text{ and } (State_{j+1} = \text{ON}) \\ U_{th,j}, & \text{if } (State_{j-1} = \text{OFF}) \text{ and } (State_{j+1} = \text{OFF}) \end{cases} \tag{5}$$

We used the algorithm similar to equation (4) at the chain ends at ( $j=1, j=N$ ). Equation (5) describes reduction of  $U_{th}$ , caused by additional heating of the channel by the value of  $\Delta T^P$  due to heating of neighbor switches at the turn-on moment, in this case the greatest reduction of  $U_{th}$  was observed when both neighbor switches were turned-on ( $State_{j-1}=\text{ON}$  and  $State_{j+1}=\text{ON}$ ). In a simplified model we suppose that thermal effect appears, only in the change of  $U_{th}$  and the value of  $\Delta$  does not depend on the durability of a low state. Indeed, our numerical modeling results [35,44] showed that  $\Delta T^P$  has low value of the stationary level output time constant ( $\sim 3$  ns for our configuration) corresponding to the durability of the current pulse front. On the other hand, temperature increase affects the value of  $U_{th}$  more than the value of  $U_h$ , therefore our approximations are physically valid.

To model the experimental two-oscillators scheme (Fig. 1c) with the distance between the switches  $d \sim 21 \mu\text{m}$  we applied the following parameters of I-V characteristic: ( $I_{th,1} = 390 \mu\text{A}$ ,  $I_{h,1} = 1100 \mu\text{A}$ ,  $U_{th,1} = 5 \text{ V}$ ,  $U_{h,1} = 1.5 \text{ V}$ ,  $U_{cf,1} = 0.8 \text{ V}$ ,  $R_{off,1} = 13 \text{ k}\Omega$ ,  $R_{on,1} = 620 \Omega$ ,  $I_{th,2} = 370 \mu\text{A}$ ,  $I_{h,2} = 1330 \mu\text{A}$ ,  $U_{th,2} = 5.4 \text{ V}$ ,  $U_{h,2} = 1.7 \text{ V}$ ,  $U_{cf,2} = 1 \text{ V}$ ,  $R_{off,2} = 14.5 \text{ k}\Omega$ ,  $R_{on,2} = 530 \Omega$ ), and for switches with  $d \sim 12 \mu\text{m}$  and further model calculations ( $I_{th,1} = 550 \mu\text{A}$ ,  $I_{h,1} = 1100 \mu\text{A}$ ,  $U_{th,1} = 5 \text{ V}$ ,  $U_{h,1} = 1.5 \text{ V}$ ,  $U_{cf,1} = 0.8 \text{ V}$ ,  $R_{off,1} = 9.1 \text{ k}\Omega$ ,  $R_{on,1} = 620 \Omega$ ,  $I_{th,2} = 450 \mu\text{A}$ ,  $I_{h,2} = 1330 \mu\text{A}$ ,  $U_{th,2} = 5.4 \text{ V}$ ,  $U_{h,2} = 1.7 \text{ V}$ ,  $U_{cf,2} = 1 \text{ V}$ ,  $R_{off,2} = 12 \text{ k}\Omega$ ,  $R_{on,2} = 530 \Omega$ ). To model long-range synchronization the switches were considered identical with the parameters corresponding to those for switch № 1 at  $d \sim 12 \mu\text{m}$ .

We assumed  $\Delta_{1 \rightarrow 2} = \Delta_{2 \rightarrow 1} = \Delta$  ( $\Delta_{j \pm 1 \rightarrow j} = \Delta_j = \Delta$ ) for all calculations, i.e. that the mutual effect of oscillators has the same value and the concrete values for each case are presented in the results section. But it could be assumed that when  $\Delta_{1 \rightarrow 2} \neq \Delta_{2 \rightarrow 1}$  or, for instance,  $\Delta_{1 \rightarrow 2} = 0$   $\Delta_{2 \rightarrow 1} \neq 0$  it is possible to model the situation of one-way interaction of one oscillator on another as it often happens in biological systems [51] and this case may become the object of further examination of this model.

### 2.3 Phase-locking estimation method

For synchronization assessment we introduced parameters of synchronization effectiveness  $\eta$  and subharmonic ratio  $SHR$  and described in detail the techniques of their calculation in one of our papers [36]. The idea of  $SHR$  may be understood as the ratio of a signal's subharmonic numbers ( $k_1, k_2$ , see Fig. 3a) at the most probable synchronization frequency  $F_s$  expressed by the formula:

$$SHR = \frac{k_2}{k_1} \quad (6)$$

In other words, equation (6) uses spectral coherence approaches to describe synchronization of the higher order  $k_2 : k_1$ , with that the following relation is observed:

$$F_s = k_1 \cdot F_1^0 = k_2 \cdot F_2^0, \quad (7)$$

where  $F_1^0, F_2^0$  are frequencies of main harmonics.

On the other hand,  $SHR$  meaning may be estimated using a phase-locking method:

$$SHR = \frac{M_1}{M_2}, \quad (8)$$

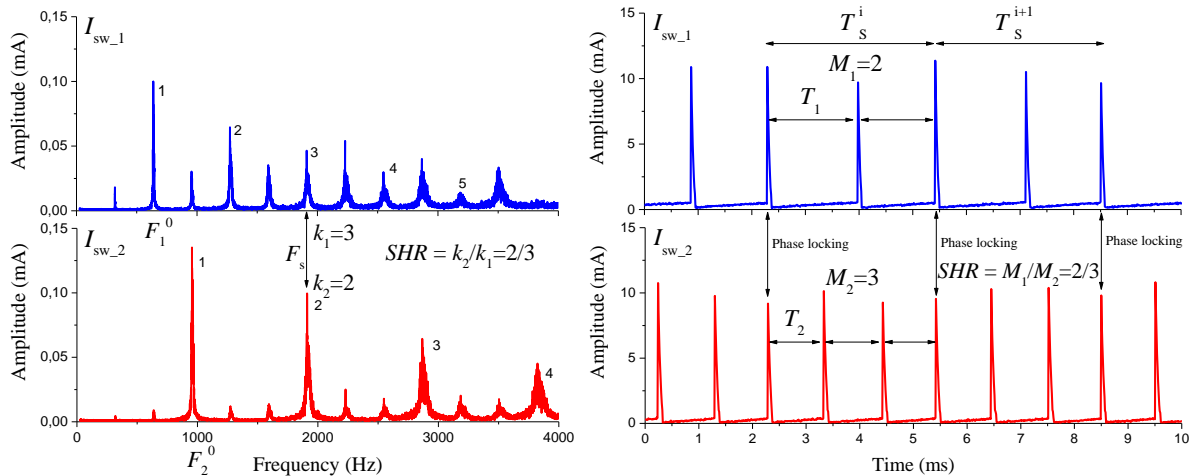
where  $M_1$  and  $M_2$  are the most probable numbers of signal periods falling into the synchronization period  $T_s^i$  of two oscillators (see Fig. 3b, where  $i$  is a conditional number of periods  $T_s$ ). Examples of spectra and current oscillogram  $I_{sw_{-1(2)}}$  in Fig. 3 correspond to a strong coupling at  $I_1=580 \mu A$ , here  $T_s^i$  is determined as the time between two moments of phase-locking current peaks occurrence. In general, especially when a system behaves erratically, synchronization periods differ and spread in  $T_s^i \neq T_s^{i+1}$  and  $M$  values so the most probable values of  $M_1$  и  $M_2$  are given in equation (8).

It is clear from equations (6, 8) that  $SHR$  varies discretely and may be presented as a common fraction (1/1, 1/2, 2/3, etc.) as ( $k_1, k_2$ ) and ( $M_1, M_2$ ) belong to a set of integers. Synchronization effectiveness  $\eta$  is determined by the minimal value of two probabilities corresponding to  $M_1$  и  $M_2$  and are expressed in percent [36].

$$\eta = \min( P(M_1), P(M_2) ) \quad (9)$$

At the final step, the values of  $\eta$  were compared with the threshold value of  $\eta_{th}=90\%$  that we have been selected. Oscillations were considered synchronized at  $\eta \geq \eta_{th}$ , if not, they were considered desynchronized (chaotic) ones. It is clear that the results will depend on the selected value of  $\eta_{th}$ ; nevertheless the general regularities presented in this work will remain the same.

An additional limitation was the one for maximal values of  $M_1$  и  $M_2$ , if they did not meet the condition ( $M_1$  or  $M_2$ )  $\leq 20$ , then the oscillations were considered desynchronized, for instance,  $SHR=50/48$ . This limitation is valid when the model implies noise level decrease to very low values tending to zero  $U_{n0} \rightarrow 0$ , however we have not obtained synchronization at harmonics of high order in real experimental systems with high noise level. This condition, as it is shown below, is closely connected with definition the maximum classification capacity  $W_C$  of the system.



(a) (b)

**Figure 3** [Color online] Experimental spectra (a) and current oscillogram (b) of two coupled oscillators clarifying the algorithm for calculating phase synchronization parameters (the conditions correspond to strong coupling at  $I_1=580 \mu\text{A}$ ).

Phase-locking estimation method, expressed by equations (8, 9), solves the task of *SHR* search much more efficiently than spectral approach (6, 7). Firstly, this is due to the fact that the algorithm is obviously resistant to period fluctuation (as we count the number of periods and the probability of their falling out, but not their durability), while in a spectrum this is expressed by line broadening and it is not always possible to find where the synchronization frequency  $F_S$  is located, besides, with the increase of subharmonic number its amplitude decreases. Secondly, determination of the synchronization effectiveness  $\eta$  and the condition ( $\eta \geq \eta_{th}$ ) allow us to clearly separate system's synchronous state from the desynchronous (chaotic) one. Thirdly, unlike a spectral method where resource-consuming FFT is applied, only operations of comparison and addition are used here thus considerably accelerating and simplifying calculations.

Presented here phase-locking estimation method may be used not only to current oscillogram but also to voltage oscillogram at switches as the key issue here is the search of time-synchronous sharp fronts responding to the structure turn on. To conclude this section we should note that synchronization of high order is a most interesting phenomenon and presented here calculation of *SHR* according to equations (8, 9) could be further developed. For instance, here we do not consider the cases when a system has two simultaneous types of synchronization with different *SHR*; this could occur when synchronization effectiveness is  $\sim 50\%$ , but the system shows two pronounced synchronization patterns.

### 3. Results

#### 3.1 Analysis of experimental results

The dynamics of a system of two thermally coupled planar oscillators (Fig. 1c) was studied realizing conditionally "strong" ( $d = 12 \mu\text{m}$ ) and "weak" ( $d = 21 \mu\text{m}$ ) coupling (see Methods for details). Current oscillations picked off the resistor  $R_1$  were considered as an output signal. We recorded the oscillation spectra of both oscillators when a parameter ( $I_1$ ) responsible for the oscillation frequency of one of them was varied. For structures with weak coupling current  $I_1$  was changed in the range of 660-820  $\mu\text{A}$ , which, in the case of no mutual thermal coupling, modified the natural oscillation frequency  $F_1^0$  from 1200 to 2000 Hz. The current of the second oscillator remained constant  $I_2 = 720 \mu\text{A}$  and the natural frequency was  $F_2^0 \sim 1550$  Hz. Figure 4a shows a set of paired spectra of current oscillations with a step of  $\Delta I_1 = 10 \mu\text{A}$ .

The spectra show that in the current range  $710 \mu\text{A} \leq I_1 \leq 750 \mu\text{A}$ , oscillators synchronize in frequency, when  $F_1 = F_2$ , and this effect is observed in the frequency range of 1550 to 1650 Hz.

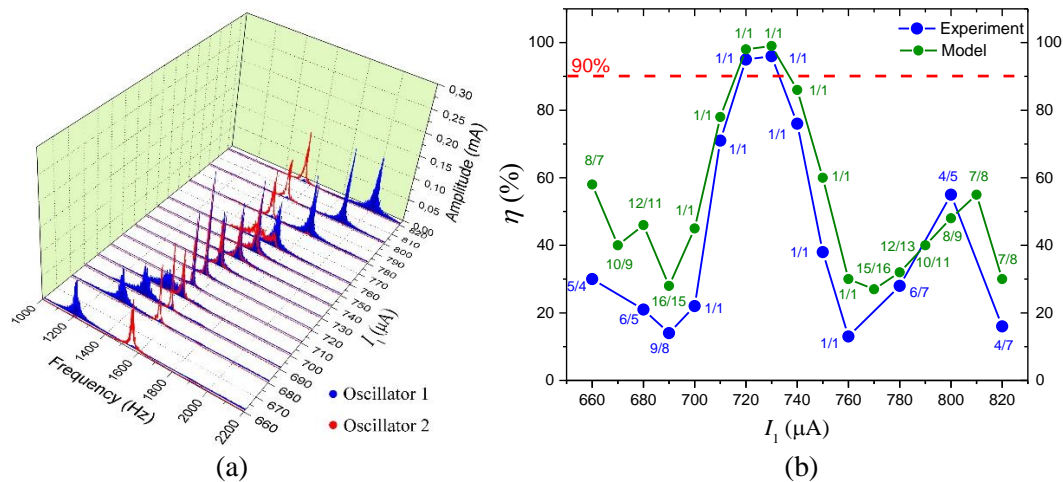
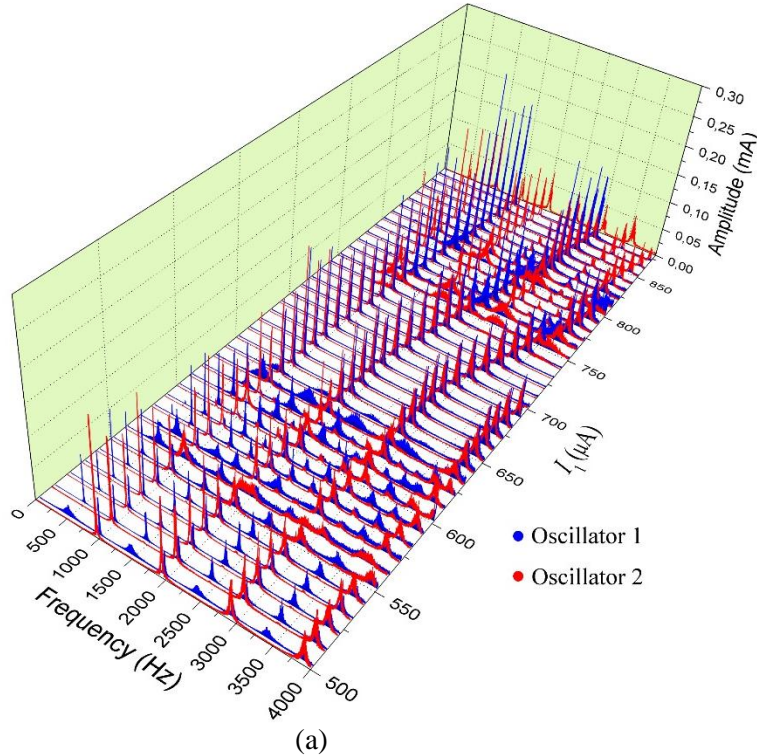


**Figure 4** [Color online] Experimental spectra of current oscillations (a) (Oscillator 1-blue graphs and Oscillator 2-red graphs), and experimental (blue graph) and model (green graph) curve  $\eta(I_1)$  (b) for weak thermal coupling

of two oscillators. Model curve  $\eta(I_1)$  was obtained at  $\Delta=0.1$  V and  $U_{n0}=20$  mV. Dashed line marks the level  $\eta_{th}=90\%$ . Fractions denote  $SHR$  values.  $I_2 = 720$   $\mu$ A.

The results of the algorithm application to calculate synchronization effectiveness  $\eta$  and  $SHR$  value for experimental oscillogram (see Methods for details) are shown in Fig. 4b (blue graph). Here we see how synchronization effectiveness changes with current  $I_1$ , and in the range  $720 \mu\text{A} < I_1 < 730 \mu\text{A}$  it exceeds the threshold value  $\eta_{th}=90\%$  when oscillations are considered synchronous ones. In the locking range  $SHR=1/1$  that complies with the conclusions made for the experimental spectra. Nevertheless, the presented numerical estimations of  $\eta$  and  $SHR$  calculated using the phase-locking estimation method (8-9) ensure more accurate estimation of synchronization state within the whole current range. We see a sharp strong peak of function  $\eta(I_1)$  corresponding to  $SHR=1/1$  and also see minimal values of  $\eta(I_1)$  that are specific to highly chaotic behavior of the system at currents  $I_1 = 700 \mu\text{A}$  and  $I_2 = 760 \mu\text{A}$ , when the broadest spectrum is observed. Besides, a weaker peak is seen at  $I_1= 800 \mu\text{A}$  ( $\eta=55\%$ ) corresponding to the most probable synchronization  $SHR=4/5$  which indicates mixed synchronization but, because of  $\eta < \eta_{th}$  we consider these oscillations as desynchronous ones. Numerical simulations of oscillogram with equations (1-4) showed that the best agreement of spectra as well as of  $\eta$  and  $SHR$  at  $I_1$  is observed at  $\Delta=0.1$  V and  $U_{n0}=20$  mV. The shape of curves in Fig. 4b has the similar form thus we may make a conclusion that model calculations of coupled oscillators' oscillogram are adequate.

At the distance between the switches  $d\sim 12 \mu\text{m}$  at strong coupling we can observe not only synchronization at first harmonic but also synchronization of higher order. Analyzing the spectrum (Fig. 5a) we can state the type of synchronization with assurance only for a few current values. For instance, it can be seen for  $I_1=520$  that the 2<sup>nd</sup> harmonic of oscillator 1 coincides with the 1<sup>st</sup> harmonic of oscillator 2 and, consequently (6),  $SHR=1/2$ . We can also see that synchronization on the first harmonic at  $SHR=1/1$  is observed in the range  $650 \mu\text{A} < I_1 < 730 \mu\text{A}$ . To determine synchronization state distribution more accurately it is necessary to use phase-locking estimation method to calculate  $SHR$ ; the results of such calculation are shown in Fig. 5b. The histogram demonstrates that there are current ranges (blue columns) with pronounced synchronization when  $SHR$  takes a number of discrete values ( $SHR=1/2, 2/3, 1/1, 4/3, 3/2$ ) and the histogram itself has a specific form known as the *devil's staircase* [1]. The broadest area belongs to  $SHR=1/1$  and the modes of desynchronous oscillations observed between the areas of strong synchronization are similar to chaotic ones ( $\eta < \eta_{th}$ , red columns, for example, for  $SHR=3/4$ ) which have predominantly frequency spread spectra.





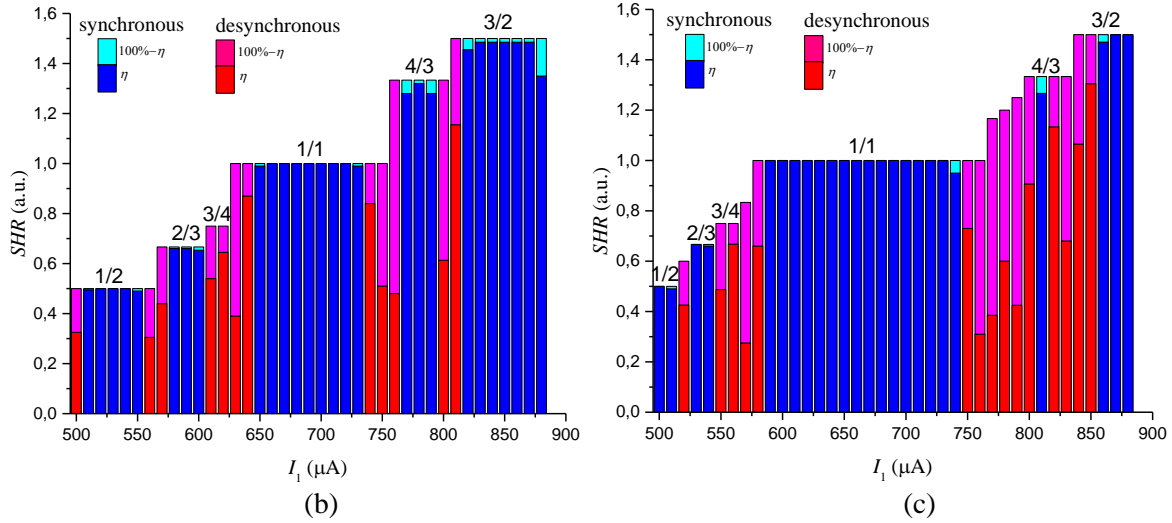


**Figure 5** [Color online] Experimental spectra (Oscillator 1-blue graphs and Oscillator 2-red graphs) as a function of  $I_1$  for strong thermal coupling of two oscillators (a). Histograms  $SHR$  having a specific form known as the *devil's staircase* [1] and corresponding to experimental (b) and model (c) data. Different colors highlight synchronous ( $\eta \geq \eta_{th}$ ) and desynchronous ( $\eta < \eta_{th}$ ) states and percentage  $\eta$  (relative to the height of the corresponding column).  $I_2 = 720 \mu A$ .

We selected parameters ( $\Delta=0.5 V$  и  $U_{n0}=20 mV$ ) for model (Eqs. (1-4)) and  $SHR$  distributions provided a histogram that was qualitatively similar to the experimental one (see Fig. 5c). The model histogram showed the same set of synchronous states and a small difference was revealed in current ranges of their occurrence and in effectiveness values, especially in the section of chaotic oscillations. It should be noted that the noise level in the model corresponded to the case with weak coupling but the level of interaction specified by  $\Delta$  increased by five times and corresponded to strong coupling.

Consequently, we have shown experimentally and by modeling the existence of the effect of high order synchronization in the two oscillators system. We have accurately estimated the ranges of synchronization occurrence and the value of  $SHR$  by using the phase-locking estimation method. We have ascertained the correlation between the numerical model and experimental results and can use this model for further research of the effect of high order synchronization.

### 3.2 Research of the system classification capacity

We suppose that the most significant result of the previous section is the discovery of an array of discrete stable states of synchronization  $N_S$  in a scheme including only two oscillators. This feature, as we have mentioned in the introduction section, may be used to classify and recognize patterns in a neural network. We have found not many variants experimentally ( $N_S=5$ ) but it is evident that  $N_S$  should depend on many parameters and we will consider this issue in the following sections. First of all it is interesting to understand how  $SHR$  are distributed in the area of control currents ( $I_1, I_2$ ). The calculation results for parameters corresponding to experimental oscillators with strong coupling ( $I_{th,1} < I_1 < I_{h,1}, I_{th,2} < I_2 < I_{h,2}$ , with current step  $\Delta I=10 \mu A$ ,  $\Delta=0.5 V$  and  $U_{n0}=20 mV$ ) are shown in Fig. 6a,c (2D and 3D images). It can be seen that 2D areas of synchronization with a certain value of  $SHR$  have the shape of *Arnold tongues* [1] (colored areas) and they are separated by areas of system's desynchronous (chaotic) behavior (black areas), and 3D distribution has the form known as the *devil's staircase* [1]. The array of synchronous states  $SHR = (1/3, 2/5, 1/2, 3/5, 2/3, 3/4, 1/1, 4/3, 3/2, 2/1, 5/2, 3/1)$  consists of  $N_S=12$ . Thus, by varying both parameters  $I_1$  and  $I_2$  it is possible to increase  $N_S$  significantly. In practice, the results shown in Fig. 5c were obtained from a cross-section of Fig. 6a at  $I_2=720 \mu A$ .

It is possible to introduce the notions of effectiveness of synchronous state  $\Psi_{SHR}$  and system synchronism level  $\Psi$  described as:

$$\Psi_{SHR} = \frac{S_{SHR}}{S} \cdot 100\%$$

$$\Psi = \sum_{N_S} \Psi_{SHR}$$
(10)

where  $S_{SHR}$  is an area occupied by a certain synchronous state, and  $S$  is the total area of space in 2D graph (Fig. 6a).

Consequently,  $\Psi_{SHR}$  determines the share of a certain synchronous state in the space of control parameters and  $\Psi$  is the effectiveness sum of all possible states of synchronization and shows the probability of synchronization occurrence in general. The larger  $\Psi$  the less is the probability of entering in the area of desynchronous oscillations at random selection of  $I_1$  и  $I_2$ . For Figure 6a we have 12 values of  $\Psi_{SHR}$  ( $\Psi_{1/1} \sim 20\%$ ,  $\Psi_{2/1} \sim 12\%$ ,  $\Psi_{1/2} \sim 6\%$ ,  $\Psi_{3/1} \sim 3\%$ ,  $\Psi_{3/2} \sim 2\%$ ,  $\Psi_{1/3} \sim 2\%$ ,  $\Psi_{4/3} \sim 1.7\%$ ,  $\Psi_{2/3} \sim 1.4\%$ ,  $\Psi_{3/4} \sim 1\%$ ,  $\Psi_{5/2} \sim 0.36\%$ ,  $\Psi_{2/5} \sim 0.3\%$ ,  $\Psi_{5/3} \sim 0.14\%$ ), and it can be seen that the highest value occurs at synchronization at the first harmonic  $SHR=1/1$ , which is reasonable due to oscillators symmetry, and the whole system synchronism is  $\Psi \sim 50\%$ .

Hereafter a question arises: how do the space distribution of  $SHR$  and value  $N_S$  depend on the coupling level  $\Delta$  and  $U_{n0}$  noise? Figures 6b,d show 2D and 3D distributions of  $SHR$  for  $\Delta=0.3$  V и  $U_{n0}=2$  mV. It can be seen that by changing  $\Delta$  and  $U_{n0}$  it is possible to increase the number of synchronization areas  $N_S=82$  and they are still linear areas with diagonal symmetry, in this case the value of  $\Psi_{SHR}$  of some states decreases and the general synchronism increases  $\Psi \sim 61\%$ . Graphs in Fig. 7 provide a more detailed answer to this question.

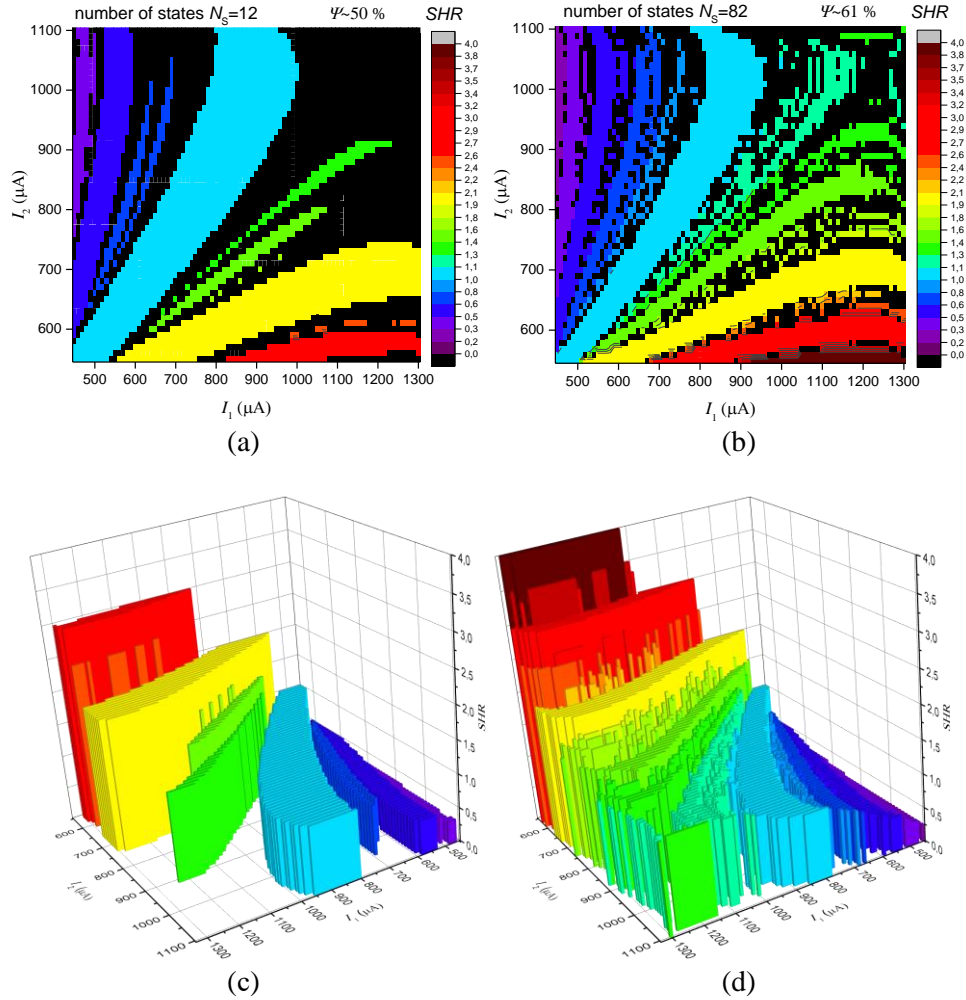


**Figure 6** [Color online] Calculation results of 2D and 3D distributions of  $SHR$  for model parameters corresponding to experimental oscillators ( $\Delta=0.5$  V и  $U_{n0}=20$  mV) (a, c) and to oscillators with parameters ( $\Delta=0.3$

V и  $U_{n0}=2$  mV) (b, d). 2D distribution of *SHR* has the form known as the *Arnold tongues*, and 3D has the form known as the *devil's staircase*.

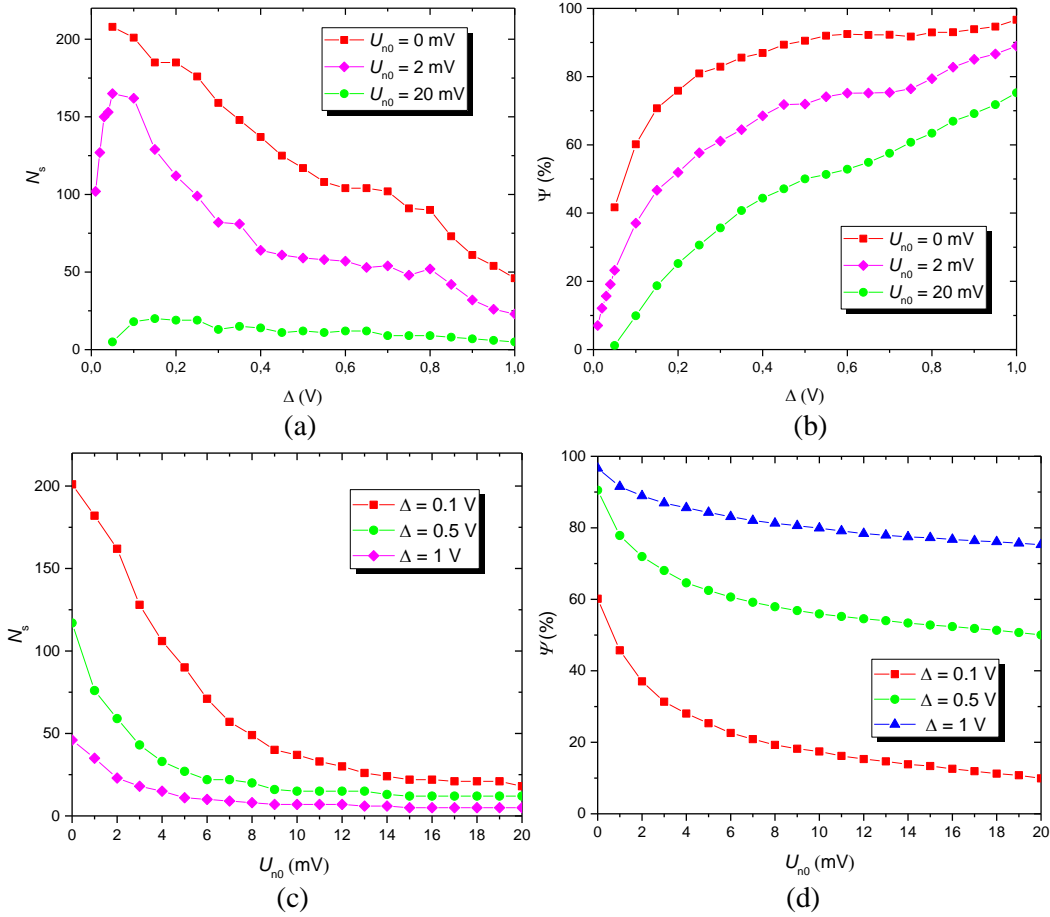


**Figure 7** [Color online] Functions of state numbers  $N_s$  (a) and system level of synchronism  $\Psi$  (b) on the value of  $\Delta$  at fixed values of noise  $U_{n0}$ ; functions of  $N_s$  (c) and  $\Psi$  (d) on noise  $U_{n0}$  at fixed values of  $\Delta$ .

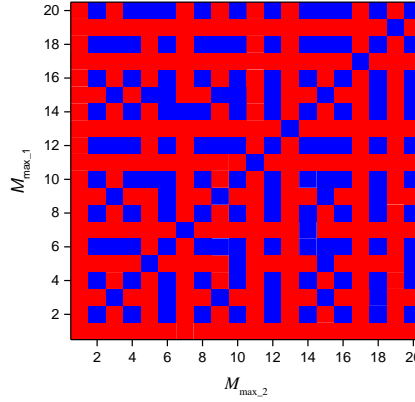
Figure 7a shows the dependence of synchronization states number  $N_s$  on the value of thermal coupling  $\Delta$  at fixed values of noise  $U_{n0}$ . For the curves where  $U_{n0} \neq 0$ , it is possible to determine the optimal value of coupling  $\Delta_{opt}$  at which maximum  $N_s$  occurs, in this case  $\Delta_{opt}$  shifts towards less values when  $U_{n0}$  decreases. It seems that the maximum occurrence is caused by the opposition of two factors: the noise that causes desynchronization, and coupling, that causes synchronization. When the coupling level changes from 0 to  $\Delta_{opt}$  the number of synchronization states  $N_s$  begins to grow sharply and further increase of  $\Delta$  results in decrease of  $N_s$ , which is connected with enlargement of synchronization areas with low order of *SHR* (for example, *SHR*=1/2) due to their integration with the areas with higher order of *SHR* (for example, *SHR*=11/20). High values of  $N_s > 150$  at low noise should be noted, and even at experimental noise level  $U_{n0}=20$  mV the maximum value is  $N_s \sim 20$  ( $\Delta_{opt}=0.15$  V), which is rather a high value for the system consisting of only two oscillators. Figure 7b shows the dependence of the system synchronization level  $\Psi$  on the value of thermal coupling at various  $U_{n0}$ . All curves show asymptotic behavior and tend to the level  $\Psi=100\%$ , in this case the system has higher  $\Psi$  at less  $U_{n0}$ . Increase of function  $\Psi(\Delta)$  is caused by the effect of occupation the areas without synchronization (Arnold's tongues broaden occupying dark areas, see Fig. 6a,b). With regard to the classification problem, the system synchronism level demonstrates the probability of objects classification in the area of control parameters variation.

Figure 7c shows the dependence of  $N_s$  on noise value  $U_{n0}$  at three levels of coupling force  $\Delta$ . All curves demonstrate the decrease of  $N_s$  when the noise amplitude increases. This may be attributed to the fact that when the noise power increases, the power corresponding to the harmonics of the highest orders becomes insufficient for oscillators synchronization. In this case the levels of synchronization of high order seem to disappear and at

maximum values of noise synchronization might remain only on the first harmonic ( $SHR=1/1$ ). It can be seen that the absolute value of the derivative  $|\partial N_s/\partial U_{n0}|$  decreases with the increase of the coupling level  $\Delta$ , this may be interpreted as the resistance increase to the noise impact.

Figure 7d presents the dependence of the system synchronization level on the value of noise  $U_{n0}$  at various levels of  $\Delta$ . It can be seen that the increase of  $\Delta$  and decrease of  $U_{n0}$  contribute to the increase of  $\Psi$ . The most substantial changes are observed at low noises  $U_{n0} < 4\text{mV}$ , this could be due to sharp change of  $N_s$  (see Fig. 7c).

As we have already mentioned in the section “phase-locking estimation method”, while calculating  $N_s$  we calculated the values of  $SHR$  when  $(M_1 \text{ and } M_2) \leq 20$ . If to present the space of possible values  $M_1$  and  $M_2$  (Fig. 8) we can see that the maximum number of possible synchronous states specified by equation (8) is  $N_s=255$ , it is equivalent to the number of red squares in the area  $(20 \times 20)$ . It should be clarified that the blue squares in Fig. 8 correspond to the states that are translations of more common fractions, for instance, from a fraction  $1/2$  fractions  $2/4, 3/6, 4/8$  and so on may be obtained but they are not taken into account at calculation. If we take synchronization absence as a separate state then the total number of states (let’s call it classification capacity  $W_C$ ) will be  $W_{C_{20}}=256$ .



**Figure 8** [Color online] Combination of resolved synchronous states (red squares) and those obtained using the translation method (blue squares) when  $(M_1 \text{ and } M_2) \leq 20$ . The total number of synchronous states is  $N_{s_{20}}=255$ .

It is easy to demonstrate that depending on the chosen limit for  $M$  the number of possible states may have the following values ( $W_{C_3}=8, W_{C_4}=12, W_{C_8}=44, W_{C_{10}}=64, W_{C_{14}}=128, W_{C_{20}}=256, W_{C_{100}}=6088$ ). If desired, an analogy with binary logic could be drawn for some values, when the capacitance of a variable depends on the bits number  $n$  and is determined as  $2^n$  (1, 2, 4, 8, 16, 32, 64, 128, 256, etc), consequently it will be possible to realize an interface between the oscillator network and computer.

### 3.3 Effect of a long-range synchronization

As we have already noted, the effect of long-range synchronization was observed in a number of papers including research of real biological neural networks, but the physical mechanism of this coupling is still the focus of researchers’ attention. A model of a one-dimensional array used in our research is shown in Figure 2b and is described by equations (1-5). From general assumptions it is clear that if there is synchronization  $SHR_{j,j+1}$  between each neighbor oscillator then the synchronization between the first and the last oscillators is described by equation:

$$SHR_{1,N} = SHR_{1,2} \cdot SHR_{2,3} \cdot \dots \cdot SHR_{N-1,N} \quad (11)$$

For example, for a three-oscillators system at certain parameters of supply current may be observed a situation when synchronization is expressed by the following sequence  $SHR_{1,3}=(1/2) \cdot (3/4)=(3/8)$ , and for a five-oscillators system  $SHR_{1,5}=(1/2) \cdot (3/4) \cdot (4/3) \cdot (2/1)=(1/1)$ . Consequently, synchronization on subharmonics enables us to synchronize outermost oscillators and realize long-range synchronization through pair synchronization of oscillators included in the coupling network. Another interesting revealed effect is the fact that there are modes of long-range synchronization when synchronization of neighbor oscillators inside the network has the effectiveness

lower than the threshold one ( $\eta < \eta_{th}$ ), i.e. they are not synchronized formally. For example, for a five-oscillators system a situation may be observed when  $SHR_{1,5}=(1/2, \eta=97\%)\cdot(3/4, \eta=50\%)\cdot(4/3, \eta=67\%)\cdot(2/1, \eta=92\%) = (1/1, \eta=97\%)$ , the effectiveness of synchronization for each pair of oscillators is given here in brackets. Thus, synchronization on subharmonics allows effective transfer of synchronization even at weak synchronization of some elements. This effect may be caused by the probability (already mentioned above) that there are some types of synchronization patterns coexisting in a signal, which transfer the interaction, although the effectiveness of the signal is technically lower than the threshold one. This effect requires further detail research and, as shown below, may be used to create logical elements for computational problems.

To research actual long-range synchronization we made calculations for long chains of oscillators in the range  $N=10-100$ , their results were practically independent of  $N$  and are shown in Figure 9 for  $N=100$ . We determined synchronization between the 1<sup>st</sup> and 100<sup>th</sup> oscillators  $SHR_{1,100}$ , while the currents varied for the outmost oscillators 1 and 2 (Fig. 9a) and central oscillators 51 and 52 (Fig. 9b), currents at all other oscillators were  $I=750 \mu A$  and the coupling levels  $\Delta=0.3 V$  between them remained constant.

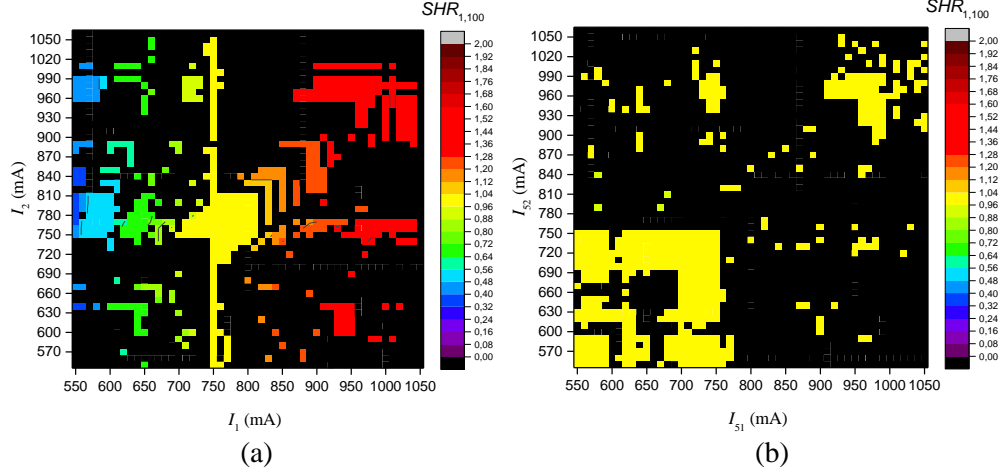


**Figure 9** [Color online] Distribution  $SHR_{1,100}$  for a long chain of oscillators ( $N=100$ ) at current variation for oscillators 1 and 2 (a) and 51 and 52 (b).

Figure 9a shows that distributions  $SHR_{1,100}$  have a change gradient only along axis  $I_1$ , unlike that for a two-oscillators scheme (Fig. 6). This is due to the fact that synchronization was measured between the 1<sup>st</sup> changed and the 100<sup>th</sup> non-changed oscillators. At the same time symmetry of synchronous states remained a diagonal one which indicates the role of mutual relation of neighbor oscillators currents for the physics of synchronism propagation along the chain, however the areas of synchronization are distributed unequally and do not form a pronounced system of Arnold's tongues.

As for Figure 9b, the distribution of one single state is  $SHR_{1,100}=1/1$ , this is obviously due to permanent frequencies of the outmost oscillators. Thus, the relation  $I_{51}$  and  $I_{52}$  acts as the key switching the synchronization on or off, and the map of switched-on states is shown in this figure. Predominantly diagonal symmetry, as in the first case, is due to equal share of changed oscillators for synchronization spreading along the chain.

### 3.4 Application of high order synchronization for computer calculations

In addition to tasks of classification, the effect of high order synchronization may be used to construct computation oscillator systems. Here we may show several approaches.

First, equation (11) actually demonstrates realization of “multiplication” operation in the oscillator chain. This approach is close to analogue computation system as it uses transformation of a physical parameter  $SHR$ .

Second, digital binary logic could be used, where the states with logical “1” or “0” may be presented as different types of mutual synchronization of oscillators. For example, is a system has two basic oscillators (Fig. 10) we denote them as oscillator 1 and oscillator 2; they are the sources of signals of two basic levels (“0”, “1”).

At least three principles of the signal splitting into logical levels may be suggested through the following equations (12-14):

$$Logic\ level = \begin{cases} "1", & \text{synchronized with oscillator 1 } (\eta \geq \eta_{th}) \\ "0", & \text{not synchronized with oscillator 1 } (\eta < \eta_{th}) \end{cases} \quad (12)$$

From equation (12) it is clear that to obtain logical “1” we should take the signal directly from oscillator 1 because it is synchronized with itself, and logical “0” should be taken from desynchronized oscillator 2 (when  $\eta < \eta_{th}$ ). If the element “NOT” passes then the desynchronized signal must become a synchronized one. This effect becomes possible because, as we have already discussed, synchronization can effectively be transferred in an oscillator chain even in case when there is no full synchronization among the chain elements.

$$Logic\ level = \begin{cases} "1", & SHR_{1,N} \text{ is finite decimal fraction} \\ "0", & SHR_{1,N} \text{ is infinite decimal fraction} \end{cases} \quad (13)$$

To clarify equation (13) it should be noted that synchronization degree  $SHR_{1,N}$  is measured between oscillator 1 and any other oscillator  $N$  (Fig. 10). The idea is that all possible combinations of  $SHR$  presented as fractions may be divided into two classes: infinite decimal fractions and finite decimal ones. Figure 10 shows an example of two elements “NOT”, a signal with synchronization  $SHR_{1,2}=1/3=0.333(3)$ , which is an infinite decimal fraction, is supplied to the input of the upper element, while a signal with  $SHR_{1,N}=1/4=0.25$ , which is a finite fraction, appears at the output. The signal received directly from oscillator 1 is always expressed as a finite fraction because  $SHR_{1,1}=1/1=1$  and corresponds to logical “1”.

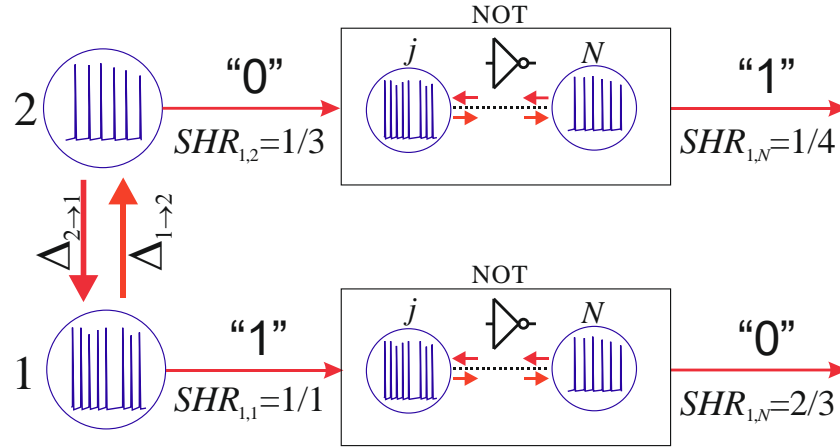


**Figure 10** [Color online] Principle scheme of logical signals sources (“1” and “0”) formed by coupled oscillators 1 and 2 and by two logical elements “NOT” functioning according to algorithm (13).

The effect of transformation from a finite fraction into an infinite one may be also be expressed by equation (11), for example,  $SHR_{1,N}=(1/3) \cdot (3/4)=(1/4)$ .

One more principle is a comparison of value  $SHR$  to some threshold value, for example, according to formula:

$$Logic\ level = \begin{cases} "1", & SHR_{1,N} \geq 1 \\ "0", & SHR_{1,N} < 1 \end{cases} \quad (14)$$

It should be noted that to realize logical elements it is necessary to select parameters of oscillators composing a logical element so that the coefficient of synchronization transfer changed as a function of the logical level of the input signal. Development of actual schemes is a challenging problem and may become a new research topic.

Consequently, we have proposed several ways of computation process based on the effect of high order synchronization, that may be defined under a general term as synchronize-based logic. Some methods (Eqs. (11-14)) may be realized strictly by describing oscillations using fractional parameter  $SHR$  and they are unsuitable for a conventional synchronization effect on first harmonic.

## 4. Discussion

Therefore, in this work we have thoroughly studied the scheme of two thermally coupled VO<sub>2</sub> oscillators and found that it demonstrates the effect of high order synchronization that may be used to create a system of pattern classification and recognition in an oscillator neural network. The specific feature of this solution is that the scheme consists of only two oscillators and its experimental realization has the state number  $N_s=12$ , besides, we have shown by modeling that it is possible to obtain much larger values  $N_s>150$  at certain levels of coupling strength  $\Delta$  and noise  $U_{n0}$ . In comparison with the study of Vodenicarevic *et al.* [5], where the scheme consisted of four oscillators and had the maximum value  $N_s=9$  due to classical synchronization effect on first harmonics, presented here method of classification on subharmonics has a distinct advantage.

Phase-locking estimation method was used to estimate the value of subharmonic ratio and synchronization effectiveness for spiking type oscillations. This method has a number of advantages and helps to solve the problem of *SHR* search much more efficiently than the spectral approach.

We have shown that the maximum theoretical classification capacity  $W_C$  of two oscillators may vary in a wide range depending on the selected parameters of the algorithm of phase-locking estimation method and it can take such values as, for example,  $W_C=(8, 64, 128, 256)$ , thus inviting the idea to develop an interface between oscillator and binary computer logic. Theoretically, at low noises  $W_C$  may have even higher values, although it is clear that actually obtained values are  $N_s < W_C$  and depend on particular parameters of the scheme that specify the area of oscillations in the circuit.

The concepts of effectiveness of synchronous state  $\Psi_{SHR}$  and synchronism level  $\Psi$  have been introduced that determine the probabilities of synchronization at a certain value of *SHR* and the probability of the system synchronization as a whole, and allow us to estimate the system applicability to solve practical tasks.

We have presented the model of thermal coupling (Eqs. (1-5)) of two oscillators, have tested it and found good agreement with experiment, this allowed modeling of the scheme and revealing the dependence of synchronization state number on coupling value and noise level. It was shown that dependence  $N_s(\Delta)$  has a maximum and noise increase always leads to  $N_s$  and  $\Psi$  decrease. Distributions of *SHR* in the area of control parameters have the shape of Arnold's tongues and represent linear areas with diagonal symmetry.

The effect of long-range synchronization has been shown when synchronization of the outmost oscillators is expressed via the multiplication (11) of intermediate elements *SHR*. Besides, we have shown a remarkable ability of chains to transfer synchronization even at low values of synchronization effectiveness of separate intermediate pairs of oscillators. This fact points to the stability of the mechanism of high order synchronization transfer at long range, this being very important for practice. It also has been shown that synchronization distribution does not form a bright picture of "Arnold's tongues", but some of oscillator pairs may play the role of a key that switches on or off synchronization of the outmost oscillators. Thus, it may be said that the presented effect of long-range synchronization allows us to unite in a single network a large number of oscillators that affect each other in a certain way through the operation of "multiplication" which in turn increases the classification capacity of a neural system as a whole and this effect requires further research.

The paper also considers possible principles of computation based on the effect of high order synchronization (synchronize-based logic), in particular, an analogue principle of multiplication and digital approach to binary calculation realization are shown.

To summarize, it must be noted that the described effects of increasing classification capacity of oscillator schemes and computation principles based on the universal effect of higher order synchronizations may be used in the majority of oscillators with any type of coupling thus enhancing the practical value of the presented results for developing spiking neural networks capabilities.

## Acknowledgements

This research was supported by Russian Science Foundation (grant no. 16-19-00135).

## References

- [1] A. Pikovsky, M. Rosenblum, J. (Jürgen) Kurths, Synchronization : a universal concept in nonlinear sciences, Cambridge University Press, 2001.

- [2] Y. Fang, V. V. Yashin, S.P. Levitan, A.C. Balazs, Pattern recognition with materials that compute, *Sci. Adv.* 2 (2016) e1601114–e1601114. doi:10.1126/sciadv.1601114.
- [3] P. Maffezzoni, B. Bahr, Z. Zhang, L. Daniel, Oscillator Array Models for Associative Memory and Pattern Recognition, *IEEE Trans. Circuits Syst. I Regul. Pap.* 62 (2015) 1591–1598. doi:10.1109/TCSI.2015.2418851.
- [4] D.E. Nikonov, G. Csaba, W. Porod, T. Shibata, D. Voils, D. Hammerstrom, I.A. Young, G.I. Bourianoff, Coupled-Oscillator Associative Memory Array Operation for Pattern Recognition, *IEEE J. Explor. Solid-State Comput. Devices Circuits.* 1 (2015) 85–93. doi:10.1109/JXCDC.2015.2504049.
- [5] D. Vodenicarevic, N. Locatelli, F. Abreu Araujo, J. Grollier, D. Querlioz, A Nanotechnology-Ready Computing Scheme based on a Weakly Coupled Oscillator Network, *Sci. Rep.* 7 (2017) 44772. doi:10.1038/srep44772.
- [6] M. Meier, R. Haschke, H.J. Ritter, Perceptual grouping through competition in coupled oscillator networks, *Neurocomputing.* 141 (2014) 76–83. doi:10.1016/J.NEUCOM.2014.02.011.
- [7] A.X. Benicasa, M.G. Quiles, T.C. Silva, L. Zhao, R.A.F. Romero, An object-based visual selection framework, *Neurocomputing.* 180 (2016) 35–54. doi:10.1016/J.NEUCOM.2015.10.111.
- [8] K. Yogendra, D. Fan, Y. Shim, M. Koo, K. Roy, Computing with coupled Spin Torque Nano Oscillators, in: 2016 21st Asia South Pacific Des. Autom. Conf., IEEE, 2016: pp. 312–317. doi:10.1109/ASPDAC.2016.7428030.
- [9] N. Shukla, W.-Y. Tsai, M. Jerry, M. Barth, V. Narayanan, S. Datta, Ultra low power coupled oscillator arrays for computer vision applications, in: 2016 IEEE Symp. VLSI Technol., IEEE, 2016: pp. 1–2. doi:10.1109/VLSIT.2016.7573439.
- [10] S. Lynch, Binary Oscillator Computing, in: *Dyn. Syst. with Appl. Using MATLAB®*, Springer International Publishing, Cham, 2014: pp. 435–455. doi:10.1007/978-3-319-06820-6\_20.
- [11] J.C. Coulombe, M.C.A. York, J. Sylvestre, Computing with networks of nonlinear mechanical oscillators, *PLoS One.* 12 (2017) e0178663. doi:10.1371/journal.pone.0178663.
- [12] N. Shukla, A. Parihar, E. Freeman, H. Paik, G. Stone, V. Narayanan, H. Wen, Z. Cai, V. Gopalan, R. Engel-Herbert, D.G. Schlom, A. Raychowdhury, S. Datta, Synchronized charge oscillations in correlated electron systems, *Sci. Rep.* 4 (2015) 4964. doi:10.1038/srep04964.
- [13] A. Parihar, N. Shukla, S. Datta, A. Raychowdhury, Computing with dynamical systems in the post-CMOS era, in: 2016 IEEE Photonics Soc. Summer Top. Meet. Ser., IEEE, 2016: pp. 110–111. doi:10.1109/PHOSST.2016.7548777.
- [14] A.A. Sharma, J.A. Bain, J.A. Weldon, Phase Coupling and Control of Oxide-Based Oscillators for Neuromorphic Computing, *IEEE J. Explor. Solid-State Comput. Devices Circuits.* 1 (2015) 58–66. doi:10.1109/JXCDC.2015.2448417.
- [15] S. Li, X. Liu, S.K. Nandi, D.K. Venkatachalam, R.G. Elliman, Coupling dynamics of Nb/Nb<sub>2</sub>O<sub>5</sub> relaxation oscillators, *Nanotechnology.* 28 (2017) 125201. doi:10.1088/1361-6528/aa5de0.
- [16] A. Kumar, P. Mohanty, Autoassociative Memory and Pattern Recognition in Micromechanical Oscillator Network, *Sci. Rep.* 7 (2017) 411. doi:10.1038/s41598-017-00442-y.
- [17] V. Flovik, F. Macià, E. Wahlström, Describing synchronization and topological excitations in arrays of magnetic spin torque oscillators through the Kuramoto model, *Sci. Rep.* 6 (2016) 32528. doi:10.1038/srep32528.
- [18] G. Csaba, W. Porod, Computational Study of Spin-Torque Oscillator Interactions for Non-Boolean Computing Applications, *IEEE Trans. Magn.* 49 (2013) 4447–4451. doi:10.1109/TMAG.2013.2244202.
- [19] R. Lebrun, S. Tsunegi, P. Bortolotti, H. Kubota, A.S. Jenkins, M. Romera, K. Yakushiji, A. Fukushima, J. Grollier, S. Yuasa, V. Cros, Mutual synchronization of spin torque nano-oscillators through a long-range and tunable electrical coupling scheme, *Nat. Commun.* 8 (2017) 15825. doi:10.1038/ncomms15825.
- [20] N. Locatelli, A. Hamadeh, F. Abreu Araujo, A.D. Belanovsky, P.N. Skirdkov, R. Lebrun, V. V. Naletov, K.A. Zvezdin, M. Muñoz, J. Grollier, O. Klein, V. Cros, G. de Loubens, Efficient Synchronization of Dipolarly Coupled Vortex-Based Spin Transfer Nano-Oscillators, *Sci. Rep.* 5 (2015) 17039. doi:10.1038/srep17039.
- [21] H. Erzgräber, S. Wiczorek, B. Krauskopf, Locking behavior of three coupled laser oscillators, *Phys. Rev. E.* 80 (2009) 26212. doi:10.1103/PhysRevE.80.026212.
- [22] F. Yoshihara, T. Fuse, S. Ashhab, K. Kakuyanagi, S. Saito, K. Semba, Superconducting qubit–oscillator



- circuit beyond the ultrastrong-coupling regime, *Nat. Phys.* 13 (2016) 44–47. doi:10.1038/nphys3906.
- [23] Q. Yu, H. Tang, J. Hu, K. Tan Chen, *Neuromorphic Cognitive Systems*, Springer International Publishing, 2017. doi:10.1007/978-3-319-55310-8.
- [24] M. Volgushev, S. Chauvette, M. Mukovski, I. Timofeev, Precise Long-Range Synchronization of Activity and Silence in Neocortical Neurons during Slow-Wave Sleep, *J. Neurosci.* 26 (2006) 5665–5672. doi:10.1523/JNEUROSCI.0279-06.2006.
- [25] J.P. Lachaux, E. Rodriguez, J. Martinerie, F.J. Varela, Measuring phase synchrony in brain signals., *Hum. Brain Mapp.* 8 (1999) 194–208. <http://www.ncbi.nlm.nih.gov/pubmed/10619414> (accessed February 19, 2018).
- [26] P. Barraza, D.M. Gómez, F. Oyarzún, P. Dartnell, Long-distance neural synchrony correlates with processing strategies to compare fractions, *Neurosci. Lett.* 567 (2014) 40–44. doi:10.1016/J.NEULET.2014.03.021.
- [27] M. Jerry, W. Tsai, B. Xie, X. Li, V. Narayanan, A. Raychowdhury, S. Datta, Phase transition oxide neuron for spiking neural networks, in: 2016 74th Annu. Device Res. Conf., IEEE, 2016: pp. 1–2. doi:10.1109/DRC.2016.7548503.
- [28] M.D. Pickett, G. Medeiros-Ribeiro, R.S. Williams, A scalable neuristor built with Mott memristors, *Nat. Mater.* 12 (2013) 114–117. doi:10.1038/nmat3510.
- [29] N. Shukla, A. Parihar, E. Freeman, H. Paik, G. Stone, V. Narayanan, H. Wen, Z. Cai, V. Gopalan, R. Engel-Herbert, D.G. Schlom, A. Raychowdhury, S. Datta, Synchronized charge oscillations in correlated electron systems, *Sci. Rep.* 4 (2015) 4964. doi:10.1038/srep04964.
- [30] A.A. Velichko, G.B. Stefanovich, A.L. Pergament, P.P. Boriskov, Deterministic noise in vanadium dioxide based structures, *Tech. Phys. Lett.* 29 (2003) 435–437. doi:10.1134/1.1579818.
- [31] M. Jerry, A. Parihar, A. Raychowdhury, S. Datta, A random number generator based on insulator-to-metal electronic phase transitions, in: 2017 75th Annu. Device Res. Conf., IEEE, 2017: pp. 1–2. doi:10.1109/DRC.2017.7999423.
- [32] G. Czanner, S. V Sarma, D. Ba, U.T. Eden, W. Wu, E. Eskandar, H.H. Lim, S. Temereanca, W.A. Suzuki, E.N. Brown, Measuring the signal-to-noise ratio of a neuron., *Proc. Natl. Acad. Sci. U. S. A.* 112 (2015) 7141–6. doi:10.1073/pnas.1505545112.
- [33] A.A. Faisal, L.P.J. Selen, D.M. Wolpert, Noise in the nervous system, *Nat. Rev. Neurosci.* 9 (2008) 292–303. doi:10.1038/nrn2258.
- [34] T. Branco, K. Staras, The probability of neurotransmitter release: variability and feedback control at single synapses, *Nat. Rev. Neurosci.* 10 (2009) 373–383. doi:10.1038/nrn2634.
- [35] A. Velichko, M. Belyaev, V. Putrolaynen, V. Perminov, A. Pergament, Modeling of thermal coupling in VO<sub>2</sub>-based oscillatory neural networks, *Solid. State. Electron.* 139 (2018). doi:10.1016/j.sse.2017.09.014.
- [36] A. Velichko, M. Belyaev, V. Putrolaynen, V. Perminov, A. Pergament, Thermal coupling and effect of subharmonic synchronization in a system of two VO<sub>2</sub> based oscillators, *Solid. State. Electron.* 141 (2018) 40–49. doi:10.1016/J.SSE.2017.12.003.
- [37] A. Velichko, M. Belyaev, V. Putrolaynen, A. Pergament, V. Perminov, Switching dynamics of single and coupled VO<sub>2</sub>-based oscillators as elements of neural networks, *Int. J. Mod. Phys. B.* 31 (2017) 1650261. doi:10.1142/S0217979216502611.
- [38] E. Lowet, M.J. Roberts, P. Bonizzi, J. Karel, P. De Weerd, Quantifying Neural Oscillatory Synchronization: A Comparison between Spectral Coherence and Phase-Locking Value Approaches, *PLoS One.* 11 (2016) e0146443. doi:10.1371/journal.pone.0146443.
- [39] A. Parihar, N. Shukla, M. Jerry, S. Datta, A. Raychowdhury, Vertex coloring of graphs via phase dynamics of coupled oscillatory networks., *Sci. Rep.* 7 (2017) 911. doi:10.1038/s41598-017-00825-1.
- [40] N. Shukla, A. Parihar, M. Cotter, M. Barth, X. Li, N. Chandramoorthy, H. Paik, D.G. Schlom, V. Narayanan, A. Raychowdhury, S. Datta, Pairwise coupled hybrid vanadium dioxide-MOSFET (HVFET) oscillators for non-boolean associative computing, in: 2014 IEEE Int. Electron Devices Meet., IEEE, 2014: p. 28.7.1–28.7.4. doi:10.1109/IEDM.2014.7047129.
- [41] Neumann John Von, Non-linear capacitance or inductance switching, amplifying, and memory organs, US2815488A, 1954. <https://patents.google.com/patent/US2815488> (accessed March 19, 2018).
- [42] J. Roychowdhury, Boolean Computation Using Self-Sustaining Nonlinear Oscillators, *Proc. IEEE.* 103

- (2015) 1958–1969. doi:10.1109/JPROC.2015.2483061.
- [43] A. Velichko, M. Belyaev, V. Putrolaynen, V. Perminov, A. Pergament, Modeling of thermal coupling in VO<sub>2</sub>-based oscillatory neural networks, *Solid. State. Electron.* 139 (2018). doi:10.1016/j.sse.2017.09.014.
- [44] A. Pergament, A. Velichko, M. Belyaev, V. Putrolaynen, Electrical switching and oscillations in vanadium dioxide, *Phys. B Condens. Matter.* (2017). doi:10.1016/J.PHYSB.2017.10.123.
- [45] S.D. Belyaev, M. A., Boriskov, P. P., Velichko, A. A., Pergament, A. L., Putrolainen, V. V., Ryabokon, D. V., Stefanovich, G. B., Sysun, V. I., Khanin, Switching Channel Development Dynamics in Planar Structures on the Basis of Vanadium Dioxide, *Phys. Solid State.* 60 (2018) 447.
- [46] A. Pergament, G. Stefanovich, A. Velichko, Relaxation oscillations in circuits containing sandwich switches based on vanadium dioxide, *Phase Transitions.* 90 (2017) 351–361. doi:10.1080/01411594.2016.1201818.
- [47] M. Belyaev, A. Velichko, V. Putrolaynen, V. Perminov, A. Pergament, Electron beam modification of vanadium dioxide oscillators, *Phys. Status Solidi.* 14 (2016). doi:10.1002/pssc.201600236.
- [48] and A.P. Andrey Velichko, Maksim Belyaev, Vadim Putrolaynen, Valentin Perminov, Thermal coupling and effect of subharmonic synchronization in a system of two VO<sub>2</sub> based oscillators, (2018).
- [49] M. Jerry, K. Ni, A. Parihar, A. Raychowdhury, S. Datta, Stochastic Insulator-to-Metal Phase Transition-Based True Random Number Generator, *IEEE Electron Device Lett.* 39 (2018) 139–142. doi:10.1109/LED.2017.2771812.
- [50] D. Somers, N. Kopell, Rapid synchronization through fast threshold modulation, *Biol. Cybern.* 68 (1993) 393–407. doi:10.1007/BF00198772.
- [51] H. Yamamoto, R. Matsumura, H. Takaoki, S. Katsurabayashi, A. Hirano-Iwata, M. Niwano, Unidirectional signal propagation in primary neurons micropatterned at a single-cell resolution, *Appl. Phys. Lett.* 109 (2016) 43703. doi:10.1063/1.4959836.